



ON THE FORMATION OF BENZOIC ACID AND HIGHER-ORDER BENZENE CARBOXYLIC ACIDS IN INTERSTELLAR MODEL ICE GRAINS

BRANDON M. MCMURTRY^{1,2}, SEAN E. J. SAITO^{1,2}, ANDREW M. TURNER^{1,2}, HARISH K. CHAKRAVARTY^{1,2}, AND RALF I. KAISER^{1,2}

¹W. M. Keck Research Laboratory in Astrochemistry, University of Hawaii at Manoa, Honolulu, HI 96822, USA

²Department of Chemistry, University of Hawaii at Manoa, Honolulu, HI 96822, USA

Received 2016 February 25; revised 2016 July 25; accepted 2016 July 25; published 2016 November 4

ABSTRACT

With a binary ice mixture of benzene (C₆H₆) and carbon dioxide (CO₂) at 10 K under contamination-free ultrahigh vacuum conditions, the formation of benzene carboxylic acids in interstellar ice grains was studied. Fourier transform infrared spectroscopy was used to probe for the formation of new species during the chemical processing of the ice mixture and during the following temperature-programmed desorption. Newly formed benzene carboxylic acid species, i.e., benzoic acid, as well as *meta*- and *para*-benzene dicarboxylic acid, were assigned using newly emerging bands in the infrared spectrum; a reaction mechanism, along with rate constants, was proposed utilizing the kinetic fitting of the coupled differential equations.

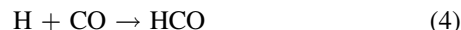
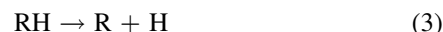
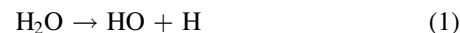
Key words: astrobiology – astrochemistry – meteorites, meteors, meteoroids – methods: laboratory: solid state

1. INTRODUCTION

During the last decade, synthetic routes leading to carboxylic acids (RCOOH)—organic molecules carrying a hydrocarbon group (R) and a carboxyl acid moiety (COOH)—in the interstellar medium (ISM) and in meteorites have attracted considerable interest from the astrochemistry, astronomy, and planetary science communities (Bernstein et al. 2002a; Pilling et al. 2011; Nuevo et al. 2014; Smith et al. 2015; Danger et al. 2016; McMurtry et al. 2016). This is due to the relevance of carboxylic acids in astrobiology as crucial biomarkers and potential reaction intermediates to form amino acids, proteins, and lipids (Schidlowski 1993; Ehrenfreund et al. 2001; Caro et al. 2002; Elsila et al. 2007; Pizzarello 2007; Koch et al. 2008). In the ISM, formic acid (HCOOH) was detected toward Sagittarius B2 (Sgr-B2) and Orion KL at fractional abundances of about 10^{−9} and about 2 × 10^{−9} with respect to molecular hydrogen (H₂) (Zuckerman et al. 1971; Liu et al. 2001); acetic acid (CH₃COOH) was probed toward Sgr-B2 and W51 at fractional abundances of (0.8–6.0) × 10^{−10} and 1.7 × 10^{−9} with respect to H₂ (Remijan et al. 2002). As fractional abundances decrease as chemical complexity rises, these findings suggest that more chemically complex carboxylic acids could also be present toward the hot core of Sgr-B2. As a matter of fact, complex carboxylic acids ranging from succinic acid to glutaric acid have been analyzed in several meteorites, such as in Murchison, Orgueil, and Tagish Lake (Remusat et al. 2005). Among these molecules, benzoic acid (C₆H₅COOH)—the prototype of an aromatic carboxylic acid—has been identified at levels of 47 ng g^{−1} in Murchison and of 100 ng g^{−1} in Orgueil (Martins et al. 2006). Benzoic acid (C₆H₅COOH) in particular represents an important intermediate in the biosynthesis of secondary metabolites, such as polyphenols, which influence the survivability of organisms (Cámara et al. 2014).

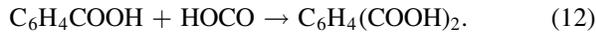
Despite the importance of carboxylic acids in extraterrestrial environments and their potential role in astrobiology as precursors to amino acids, their formation routes are still not fully understood. Carboxylic acids have been suggested to be formed on interstellar ices via the interaction of ionizing radiation in the form of ultraviolet light (UV) and galactic cosmic ray particles (GCRs). Bennett et al. (2011)

demonstrated that the exposure of water (H₂O)—carbon monoxide (CO) ices to energetic electrons can lead to the formation of formic acid at levels of 1.5% at averaged doses of 1.4 ± 0.2 eV per molecule. The authors also elucidated the formation of acetic acid (CH₃COOH) in electron-irradiated methane (CH₄)—carbon dioxide (CO₂) ices (Bennett & Kaiser 2007). Later, Kim & Kaiser (2010) demonstrated that alkyl carboxylic acids can also be synthesized efficiently at levels of up to 39% in alkane-doped carbon dioxide ices via radical–radical mediated reactions involving the hydroxycarbonyl (HOCO) radical. In all mechanisms, the interaction of the energetic electron was found to lead to oxygen–hydrogen (reaction (1)) and carbon–hydrogen (reactions (2), (3)) bonds upon the decomposition of water, methane, and a generic hydrocarbon, respectively. The released hydrogen atoms have excess kinetic energy of a few electron volts and can overcome the barrier of addition to carbon monoxide (CO) and carbon dioxide (CO₂) forming the formyl (HCO) and hydroxycarbonyl (HOCO) radical, respectively (reactions (4) and (5)). If the geometry is favorable, barrier-less radical–radical recombination processes can lead to the formation of formic acid (6), acetic acid (7), and alkyl carboxylic acids (8).



In analogy to these processes, the benzene (C₆H₆) molecule may fragment upon exposure to ionizing radiation via carbon–hydrogen loss to a phenyl radical (C₆H₅) plus atomic hydrogen, reaction (9), followed by reaction (5), and recombination of the phenyl with the hydroxycarbonyl radical (reaction (10)). In an analogous process, benzoic acid may undergo hydrogen loss from the phenyl moiety (reaction (11)) to produce a HOCO radical via reaction (5), which may then recombine with the

benzoic acid radical (C_6H_4COOH) to yield a dicarboxylic acid ($C_6H_4(COOH)_2$).



Polycyclic aromatic hydrocarbons (PAHs), similar to carboxylic acids, have been heavily studied in astrochemical settings (Oomens et al. 2003; Rhee et al. 2007; Tielens 2008). This class of compounds has attracted significant attention due to its identification within the ISM, contributing up to 30% of the galactic carbon budget (Ehrenfreund & Charnley 2000). As a result, the mechanism of formation has been well studied, where single-collision, gas-phase reactions of the phenyl radical (C_6H_5) and vinylacetylene have been shown to afford the simplest PAH, naphthalene (Parker et al. 2012). Additionally, a theoretical study by Landera et al. (2011) has shown that addition of the ethynyl radical (C_2H) to styrene may also lead to the formation of naphthalene. Bernstein et al. (2002b) provided evidence that aromatic carboxylic acids can be formed in low-temperature ices exposed to UV light. In these experiments, a carboxylic side group addition to PAHs, such as coronene ($C_{24}H_{12}$), in carbon dioxide matrices was studied. Gas chromatography–mass spectrometry of the residue identified coronene carrying a carboxyl group ($C_{24}H_{11}COOH$). However, since the products were analyzed *ex situ* via chromatographic techniques, no reaction mechanism(s) could be provided.

Here, we present a proof-of-concept study illustrating that the simplest aromatic carboxylic acid (benzoic acid (C_6H_5COOH)), along with dicarboxylic acids, can be formed in apolar interstellar analog ices containing benzene and carbon dioxide via interaction with ionizing radiation in the form of energetic electrons at temperatures as low as 10 K. Note that carbon dioxide represents a common constituent of interstellar ices at levels of 9% to 37% with respect to water (Whittet et al. 2007). Benzene—although not monitored yet in interstellar ices—has been detected in the circumstellar envelope of the planetary nebula CRL 618 via the short-wavelength spectrometer onboard the *Infrared Space Observatory* (Cernicharo et al. 2001). Laboratory experiments also demonstrated that benzene can be formed in methane (CH_4)-based ices upon interaction with GCRs (Kaiser & Roessler 1997)—methane being present in interstellar ices at levels between 1% and 4% relative to water (Gibb et al. 2004).

2. EXPERIMENTAL

The experiments were carried out in a contamination-free ultrahigh vacuum chamber evacuated to pressures of typically 5×10^{-11} Torr exploiting a magnetically suspended turbo pump (Osaka TG420MCAB), which was backed by an oil-free scroll pump (Anest Iwata ISP-500) (Bennett et al. 2004). A polished silver wafer was interfaced via indium foil and an oxygen-free high-conductivity copper target, which was located in the center of the chamber. The target was connected to a two-stage closed-cycle helium refrigerator (CTI-Cryogenics 9600) and a programmable temperature controller via a 50Ω cartridge heater capable of regulating temperatures between 10 and 330 K with an accuracy of ± 0.3 K. The ice layers were prepared by vapor deposition of premixed gases.

Here, a benzene (C_6H_6)–carbon dioxide (CO_2) gas mixture was prepared by subsequent additions of 1 mbar of benzene (C_6H_6 , Fisher Scientific, 99.99% anhydrous) and 99 mbar carbon dioxide (CO_2 , Airgas, 99.999%), which were introduced in an external gas-mixing chamber. Benzene was purified by distillation and by three consecutive freeze–thaw cycles with liquid nitrogen. This gas mixture was then introduced into the main chamber via a precision leak valve connected to a glass capillary array for 25 minutes at a pressure of 5×10^{-8} Torr. The thickness of the ice was determined to be 600 ± 60 nm *in situ* via laser interferometry (Zhou et al. 2014). Briefly, two helium–neon (HeNe) lasers (632.8 nm) were reflected off the silver wafer toward two separate photodiodes with narrow bandpass filters. The light from the 632.8 nm lasers was reflected at angles of 10° and 11.5° relative to the surface normal. The intensity of the laser light was monitored by the photodiodes as a function of time throughout the deposition process.

Prior to the irradiation, near-infrared ($10,000$ – 2000 cm^{-1}) and mid-infrared (6000 – 400 cm^{-1}) spectra were recorded for the pristine ice using a Nicolet 6700 FTIR spectrometer. Figure 1 depicts the mid-infrared spectrum of the deposited ice prior to the irradiation along with the vibrational assignments based upon literature data on benzene and carbon dioxide (Table 1). Most notably, the $\nu_1 + \nu_2$, ν_3 , and ν_2 absorptions of carbon dioxide (3800 – 3550 , 2500 – 2300 , and 700 – 650 cm^{-1}) correspond closely to the interstellar-model ices studied by Bennett et al. (2009). Likewise, evidence for the carbon–hydrogen (C–H) and aromatic ring stretches of benzene are apparent in the 3150 – 3000 and 1500 – 1000 cm^{-1} regions, respectively, aligning with the literature values of benzene (Hollenberg & Dows 1962). The relative abundance of the two starting materials was determined via a modified Beer–Lambert law (Brucato et al. 2006). For carbon dioxide, the average column density was determined based on the integrated areas of $\nu_1 + \nu_3$ and $2\nu_2 + \nu_3$ of CO_2 and ν_3 of $^{13}CO_2$, along with their corresponding absorption coefficients of 1.4×10^{-18} cm molecule $^{-1}$, 4.5×10^{-19} cm molecule $^{-1}$, and 7.8×10^{-17} cm molecule $^{-1}$, respectively (Gerakines et al. 1995). From this, the average column density of carbon dioxide in the ice mixture was found to be $(3.06 \pm 0.07) \times 10^{17}$ molecule cm^{-2} . Using the ν_{19} of C_6H_6 , with an integrated absorption coefficient of 1.5×10^{-18} cm molecule $^{-1}$ (Zhou et al. 2010), we determined the column density of benzene in the deposited ice to be $(6.5 \pm 0.2) \times 10^{15}$ molecule cm^{-2} , which corresponds to a relative abundance of 50:1 (CO_2/C_6H_6), i.e., a benzene-doped carbon dioxide ice.

The ice mixture was then irradiated for one hour with 5 keV electrons at a current of 100 nA from a Specs EQ 22-35 electron gun with an extraction coefficient of the electrons of 78.5% by scanning the electron beam over an area of the ice of 3.7 ± 0.3 cm^2 at an angle of incidence of 15° relative to the surface normal. The electron trajectories and energy losses in the ice were simulated by the CASINO code (Drouin et al. 2007). These calculations yielded a deposited energy of 4.37 keV per electron at an average penetration depth of 460 ± 10 nm, which translates to an average dose of 3.8 ± 0.5 eV per molecule in the ice. The irradiated ice was kept at 8 K for one hour and then warmed up to 300 K at a rate of 0.5 K min^{-1} . *In situ* FTIR data were collected throughout the irradiation and the temperature-programmed desorption (TPD) studies.

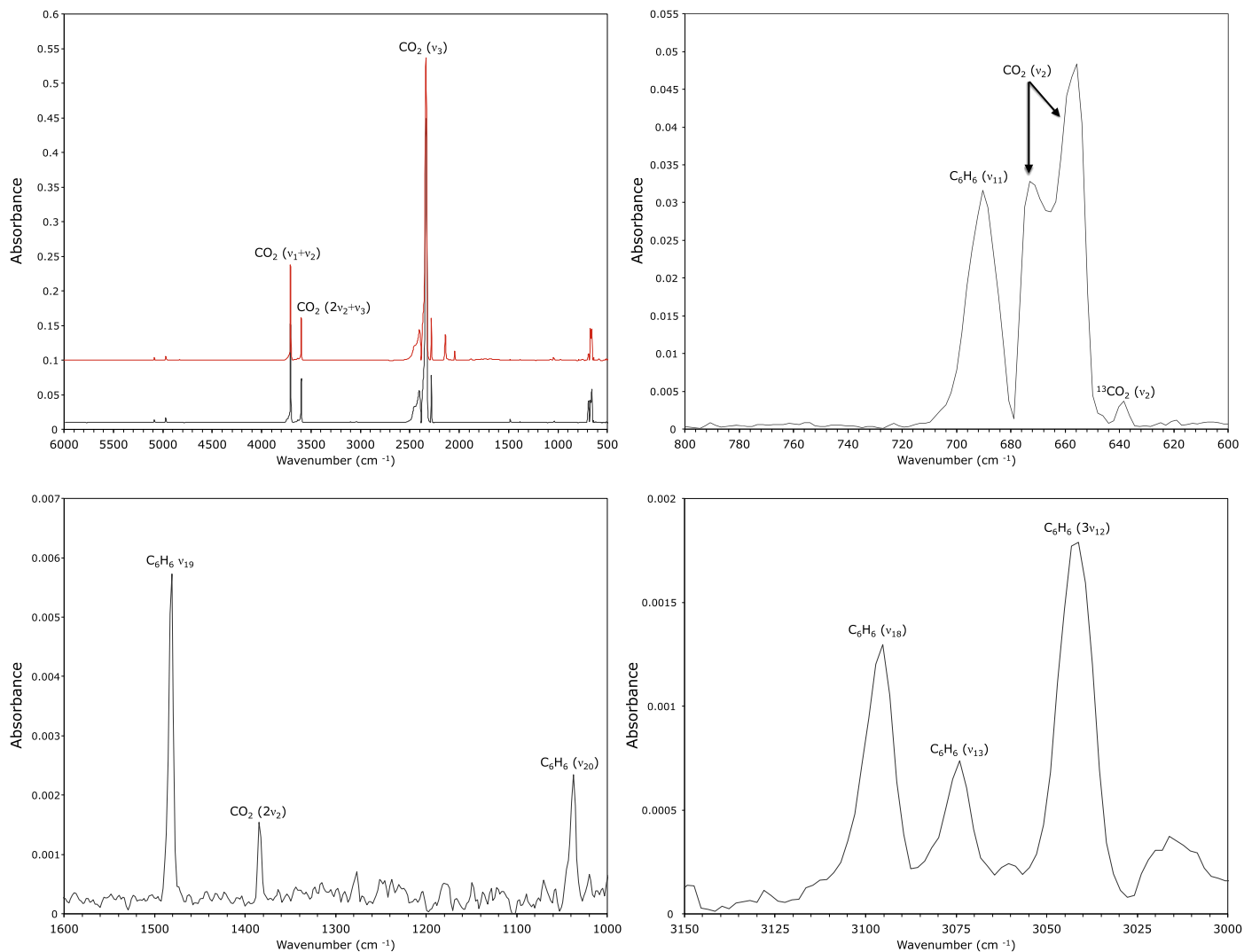


Figure 1. Mid-infrared spectra of solid benzene (C_6H_6) and carbon dioxide (CO_2) ice before irradiation at 10 K (black). The top left spectrum displays the full spectral range of $6000\text{--}500\text{ cm}^{-1}$ with the irradiated ice shown in red. The remaining three panels depict zoomed-in regions of the full spectrum. The assignment of peaks corresponding to the two starting materials is displayed on each graph.

3. RESULTS

3.1. Infrared Spectroscopy

3.1.1. Qualitative Analysis

Evidence for the radiation-induced formation of new species in the model ice was confirmed on the basis of a series of novel bands present in the ice mixture following bombardment with energetic electrons. Figure 2 displays selected regions of the infrared spectrum for the processed ice and during the subsequent TPD phase at 180, 250, and 300 K. These temperatures were selected specifically to analyze the ice mixture following the sublimation of volatile species including carbon dioxide and the low-mass species CO, CO_3 , and O_3 at 180 K, benzene at 250 K, and a residue at 300 K. For each spectrum, the absorption features were deconvoluted by exploiting Gaussian peak profiles. Particular interest is directed to spectral regions associated with peaks characteristic to benzene carboxylic acids, specifically from $1950\text{--}850\text{ cm}^{-1}$. A comprehensive summary of novel absorption features along with literature values for the assigned species is presented in Table 2. Emerging bands associated with benzoic acid

(C_6H_5COOH), benzene dicarboxylic acids ($C_6H_4(COOH)_2$), carbon monoxide (CO), carbon trioxide (CO_3), and ozone (O_3) were detected within the infrared spectrum of the electron-irradiated ice. Specifically, we find evidence for the formation of carbon monoxide and carbon trioxide based on absorptions at 2141 cm^{-1} and 2044 cm^{-1} , which correspond to the fundamental of carbon monoxide and the ν_1 ($[C=O]$ stretch) of carbon trioxide. These assignments are in good agreement with a study conducted by Bennett et al. (2004) on the irradiation of carbon dioxide ices, where CO was assigned to 2139 cm^{-1} and the ν_1 of CO_3 was assigned to 2044 cm^{-1} . Additionally, in the present study, the ν_3 of O_3 was assigned to 1042 cm^{-1} on the basis of a previous study on the formation of ozone in interstellar ices that assigned the band to 1037 cm^{-1} (Bennett et al. 2010).

In the processed ice at 10 K, features corresponding to benzoic acid (C_6H_5COOH), *m*-benzene dicarboxylic acid (*p*- $C_6H_5(COOH)_2$), and *p*-benzene dicarboxylic acid (*p*- $C_6H_5(COOH)_2$) were unambiguously identified. Specifically, the benzoic acid dimer was assigned as the carrier for bands observed at 1735 cm^{-1} ($C=O$ stretch) and 1671 cm^{-1} ($C=O$ stretch). The first assignment was determined based on a

Table 1
Assignment of Vibrational Modes in Pristine Benzene–Carbon Dioxide Ice ($C_6H_6-CO_2$) at 8 K

Absorption (cm^{-1})	Literature Value (cm^{-1})	Assignment	Characterization
5087, 4971, 4831	...	CO_2	Combinations and Overtones
3708	3700 ^a	$\nu_1 + \nu_3 CO_2$	Combination
3600	3600 ^a	$2\nu_2 + \nu_3 CO_2$	Combination
3096	3091 ^b	$\nu_{18} C_6H_6$	C–H Stretch
3075	3067 ^b	$\nu_{13} C_6H_6$	C–H Stretch
3042	3030 ^b	$3\nu_{12} C_6H_6$	Overtone
2443	2456 ^b	$\nu_{14} + \nu_{15} C_6H_6$	Combination
2335	2342 ^a	$\nu_3 CO_2$	Asymmetric Stretch
2280	2282 ^a	$\nu_3 {}^{13}CO_2$	Asymmetric Stretch
2043	2041 ^b	$\nu_{12} + \nu_{20} C_6H_6$	Combination
1831	1824 ^b	$\nu_{11} + \nu_{15} C_6H_6$	Combination
1482	1479 ^b	$\nu_{19} C_6H_6$	Ring Stretch
1384	1384 ^a	$2\nu_2 CO_2$	Overtone
1038	1038 ^b	$\nu_{20} C_6H_6$	C–H Bend
690	681 ^b	$\nu_{11} C_6H_6$	C–H Bend
672, 655	667, 665 ^a	$\nu_2 CO_2$	In-plane/Out-of- plane Bend
639	638 ^a	$\nu_2 {}^{13}CO_2$	In-plane/Out-of- plane Bend

Notes.

^a Bennett et al. (2011).

^b Hollenberg & Dows (1962).

study of benzoic acid monomers and dimers in an argon matrix which assigned the carbonyl stretch of the benzoic acid dimer to 1738 cm^{-1} . The second position was confirmed by a vibrational spectroscopic study conducted on benzoic acid (Brittain 2009) that depicted a peak linked to the benzoic acid dimer at 1678 cm^{-1} . For the *meta*-benzene dicarboxylic acid, a band at 1611 cm^{-1} (ν_{8a}) in the infrared spectrum at 8 K and a band at 1471 cm^{-1} (ν_{19b}) in the spectrum at 180 K were unambiguously assigned to ring stretches in the aforementioned species. This was confirmed by a study on the infrared spectra of the three benzene dicarboxylic acids in KBr pellets (Arenas & Marcos 1980). Arenas & Marcos (1980) assigned the ν_{8a} and ν_{19b} of *meta*-benzene dicarboxylic acid to 1610 cm^{-1} and 1485 cm^{-1} , respectively. Additionally, *para*-benzene dicarboxylic acid was attributed to an observed band at 1639 cm^{-1} ($\nu(C=O) + \delta(COH)$) based on a combined experimental and theoretical study on the infrared spectrum of *para*-benzene dicarboxylic acid (Hollauer et al. 2001). The aforementioned study assigned the $\nu(C=O) + \delta(COH)$ combination band to 1630 cm^{-1} . Assignment of the remaining newly emerging bands was accomplished using a study on the literature infrared spectra of the three benzene dicarboxylic acids (Arenas & Marcos 1980). However, it is to be noted that two broad peaks, at 1776 cm^{-1} and 1793 cm^{-1} , in the spectrum at 8 K did not correspond to a single carrier. Rather, the bands were assigned to a combination of carbonyl stretches from the various carboxylic acid species in the ice.

3.1.2. Quantitative Analysis

From the peak assignments in Section 3.1.1, the column density changes throughout the irradiation can be determined for the two reactants, benzene and carbon dioxide, along with

the irradiation-induced products. For carbon dioxide, the temporal development of the $\nu_1 + \nu_3$ and $2\nu_2 + \nu_3$ of CO_2 and the ν_3 of ${}^{13}CO_2$ was monitored to quantify the carbon dioxide molecules destroyed. Exploiting the integrated absorption coefficients of the three previously mentioned bands, $1.4 \times 10^{-18}\text{ cm molecule}^{-1}$ for the $\nu_1 + \nu_3$ of CO_2 , $4.5 \times 10^{-19}\text{ cm molecule}^{-1}$ for the $2\nu_2 + \nu_3$ of CO_2 , and $7.8 \times 10^{-17}\text{ cm molecule}^{-1}$ for the ν_3 of ${}^{13}CO_2$, we found that $(1.9 \pm 0.9) \times 10^{16}\text{ molecule cm}^{-2}$ of carbon dioxide was destroyed over the course of the hour-long irradiation. Corresponding to the diminishing carbon dioxide column density were new bands assigned to carbon dioxide and carbon trioxide. The development of the two new carbon oxides was monitored using the fundamental band of carbon monoxide, assigned to 2141 cm^{-1} , and the ν_1 of carbon trioxide, assigned to 2044 cm^{-1} . Using a previously published work on the irradiation of carbon dioxide ices (Bennett et al. 2004), we found that the integrated absorption coefficients of the two previously mentioned carbon monoxide and carbon trioxide bands to be $1.1 \times 10^{-17}\text{ cm molecule}^{-1}$ and $3.1 \times 10^{-17}\text{ cm molecule}^{-1}$, respectively. Utilizing this information, we determined that following irradiation with energetic electrons, the total increase in column density of carbon monoxide was $(1.1 \pm 0.1) \times 10^{16}\text{ molecule cm}^{-2}$, while the total increase of carbon trioxide was $(7.9 \pm 0.3) \times 10^{14}\text{ molecule cm}^{-2}$. The total column density of newly formed low-mass carbon species was therefore $(1.2 \pm 0.1) \times 10^{16}\text{ molecule cm}^{-2}$, i.e., $64 \pm 3\%$ of the total carbon dioxide destroyed was converted to carbon monoxide and trioxide. The difference between this value and the total quantity of carbon dioxide destroyed was therefore the amount reacted to form benzene carboxylic acids, i.e., $(6.8 \pm 1.0) \times 10^{15}\text{ molecule cm}^{-2}$.

The destruction of benzene was monitored by the development of its ν_{11} band at 690 cm^{-1} , with an integrated absorption coefficient of $1.5 \times 10^{-18}\text{ cm molecule}^{-1}$ (Zhou et al. 2010). Comparing the initial column density of benzene with the column density following irradiation, we found that $(4.4 \pm 0.2) \times 10^{15}\text{ molecule cm}^{-2}$ benzene molecules were destroyed upon exposure to energetic electrons. Since no other carriers containing benzene were identified in the infrared spectrum of the processed ice, it can be concluded that all benzene molecules destroyed in the hour-long irradiation were converted to benzene carboxylic acids. We therefore established the upper limit of the benzene carboxylic acid column density to be $(4.4 \pm 0.2) \times 10^{15}\text{ molecule cm}^{-2}$. Completion of the mass balance for the irradiated ice required a determination of the average number of carboxyl groups incorporated into each newly formed carboxylic acid. Using the proposed reaction, we determined the average number of carboxyl groups was equal to the column density of destroyed carbon dioxide divided by the upper limit of the carboxylic acid column density. Here we found that an average of 1.5 ± 0.4 carbon dioxide molecules were incorporated into each benzene carboxylic acid molecule formed. These findings are consistent with the assignment of a suite of mono- and disubstituted benzene carboxylic acid species within the irradiated ice as outlined above.

4. DISCUSSION

Having characterized the newly formed molecules within the processed benzene–carbon dioxide ice, we now attempt to

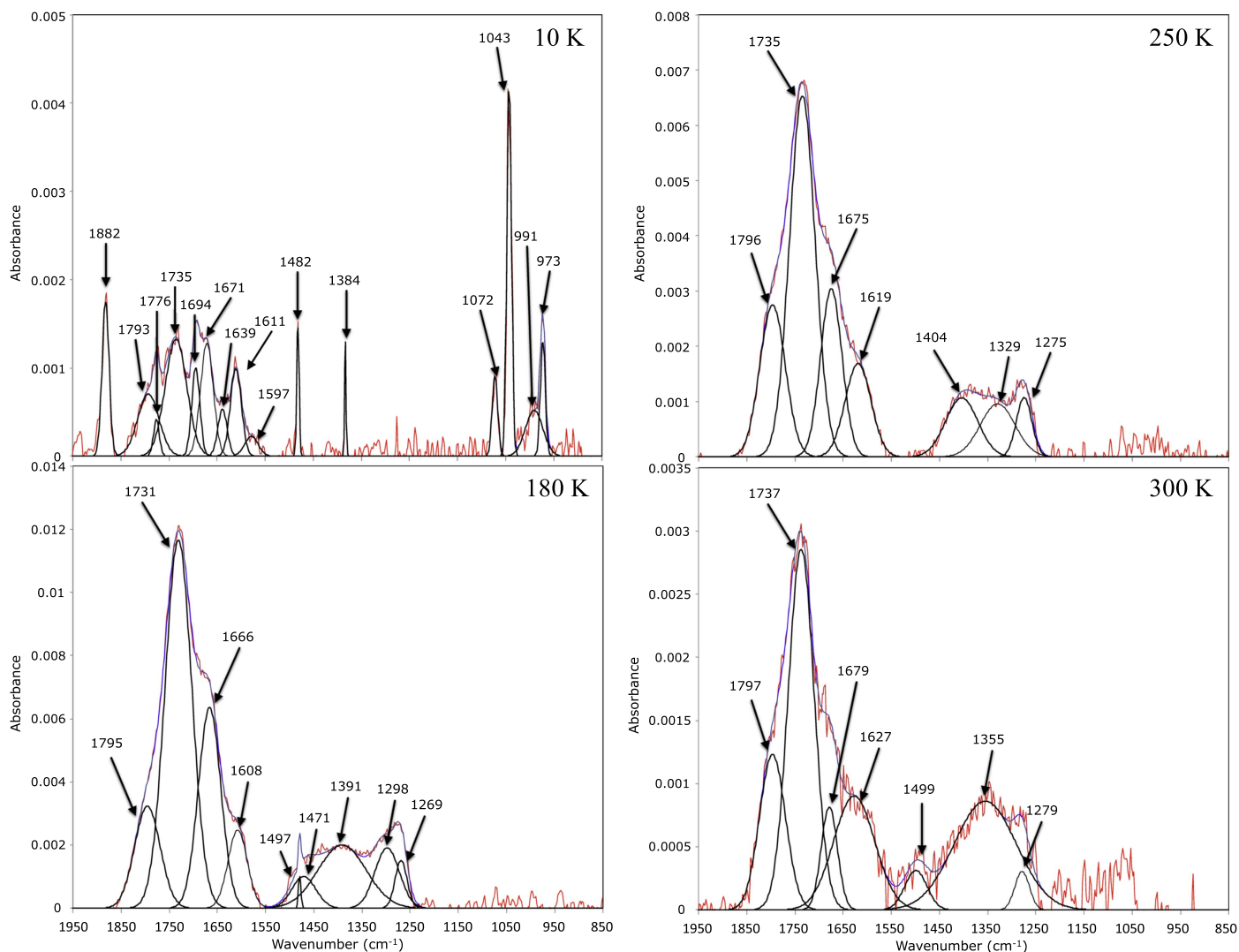


Figure 2. Deconvoluted infrared spectra of the ice following irradiation with energetic electrons at 10, 180, 250, and 300 K. The red lines correspond to experimentally collected infrared spectra, the black lines correspond to the deconvoluted fits of structures within the ice, and the blue lines correspond to the sum of the deconvoluted fittings. Absorption features assigned to radiation products are labeled by wavenumber.

elucidate the reaction mechanism involved in the production of the identified irradiation-induced species. From previous studies on carboxylic acid formation in interstellar ices (Kim & Kaiser 2010) it can be deduced that the initial step toward benzene carboxylic acid formation is hydrogen loss from the benzene molecule (reaction (9)), a reaction that is endoergic by 473 kJ mol^{-1} (4.902 eV). The released hydrogen atoms may have up to a few eV of kinetic energy (Bennett & Kaiser 2007). Hydrogen atoms possessing sufficient energy may overcome the 106 kJ mol^{-1} (1.10 eV) entrance barrier and react with carbon dioxide to form the *trans*-carboxyl radical (HOCO (reaction (5))). From here, the newly formed radicals may undergo radical–radical recombination to form benzoic acid. Subsequently, the newly formed benzoic acid molecule may undergo a second hydrogen loss from the phenyl ring upon interaction with ionizing radiation, prompting the formation of a benzene dicarboxylic acid upon recombination with a HOCO radical. However, due to the facile conversion of HOCO to carboxylic acids, a pseudo-first-order kinetic law formally via a benzene–carbon dioxide complex is considered in reactions

((13)–(14)) of radicals to benzene carboxylic acids.



These reaction pathways were also verified by kinetically fitting the temporal evolution of the column densities (Figure 3). The temporal evolution of the observed benzene carboxylic acids can be modeled by either a pseudo-first-order $A \rightarrow B$ pathway—for benzoic acid—or a consecutive mechanism $A \rightarrow B \rightarrow C$ —for benzene dicarboxylic acids:

$$[\text{C}_6\text{H}_5(\text{COOH})]_t = a(1 - e^{-k_1 t}) \quad (15)$$

$$[\text{C}_6\text{H}_4(\text{COOH})_2]_t = b \left(1 - \frac{k_3}{k_3 - k_2} e^{-k_2 t} - \frac{k_2}{k_3 - k_2} e^{-k_3 t} \right). \quad (16)$$

For fitting of the band assigned to benzoic acid, we found the rate constant for the addition of a carbon dioxide molecule to benzene to be $k_1 = (2.8 \pm 1.1) \times 10^{-4} \text{ s}^{-1}$. Normalized peak areas were used since bands assigned to dimers can have up to

Table 2
Infrared Absorption Features of the Irradiated Benzene–Carbon Dioxide Ice (C₆H₆–CO₂) at 8 K and throughout TPD

Absorptions After Irradiation ^a 8 K	Absorptions During TPD Phase ^a			Assignment			
	180 K	250 K	300 K	Wavenumber (cm ⁻¹)	Molecule	Vibration	Characterization
2141	2133	2139b	CO	ν_1	Fundamental
2044	2041 ^b	CO ₃	ν_1	C=O Stretch
1882	1879 ^b	CO ₃	...	Fermi Resonance
1793, 1776	1795	1796	1797	C=O Stretches
1735	1731	1735	1737	1738 ^c	C ₆ H ₅ (COOH)	...	Dimer C=O Stretch
1694	1687 ^d	<i>o</i> -C ₆ H ₄ (COOH) ₂	...	C=O Stretch
				1690 ^d	<i>m</i> -C ₆ H ₄ (COOH) ₂	...	C=O Stretch
1671	1666	1675	1679	1678 ^e	C ₆ H ₅ (COOH)	...	Dimer C=O Stretch
1639	1627	1630 ^f	<i>p</i> -C ₆ H ₄ (COOH) ₂	$\nu(\text{C=O}) + \delta(\text{COH})$	Combination
1611	1608	1619	...	1610 ^f	<i>m</i> -C ₆ H ₄ (COOH) ₂	ν_{8a}	Ring Stretch
1597	1590 ^c	C ₆ H ₅ (COOH)	ν_{8a}	Ring Stretch
				1590 ^d	<i>o</i> -C ₆ H ₄ (COOH) ₂	ν_{8b}	Ring Stretch
...	1497	...	1499	1496 ^e	C ₆ H ₅ (COOH)	ν_{19a}	Ring Stretch
				1496 ^d	<i>o</i> -C ₆ H ₄ (COOH) ₂	ν_{19b}	Ring Stretch
...	1471	1485 ^d	<i>m</i> -C ₆ H ₄ (COOH) ₂	ν_{19b}	Ring Stretch
...	1391	1404	...	1383 ^c	C ₆ H ₅ (COOH)	...	C–H Bend
				1402 ^d	<i>o</i> -C ₆ H ₄ (COOH) ₂	...	O–H Deform
				1387 ^c	<i>p</i> -C ₆ H ₄ (COOH) ₂
...	1298	1329	1355	1347 ^c	C ₆ H ₅ (COOH)	...	Dimer C–H Bend
...	1269	1275	1279	1275 ^c	C ₆ H ₅ (COOH)	...	Ring Stretch
				1280 ^d	<i>o</i> -C ₆ H ₄ (COOH) ₂	...	C–O Stretch
				1277 ^d	<i>m</i> -C ₆ H ₄ (COOH) ₂	...	C–O Stretch
				1280 ^d	<i>p</i> -C ₆ H ₄ (COOH) ₂	...	C–O Stretch
1072	1072 ^c	C ₆ H ₅ (COOH)	...	In-plane C–H Mode
				1069 ^d	<i>o</i> -C ₆ H ₄ (COOH) ₂	ν_{9b}	C–H Deform
1043	1037 ^b	O ₃	ν_3	Asymmetric Stretch
991	992	1000 ^c	C ₆ H ₅ (COOH)	...	C–C Stretching
				1001 ^d	<i>o</i> -C ₆ H ₄ (COOH) ₂	ν_5	C–H Out-of-plane
				1000 ^d	<i>m</i> -C ₆ H ₄ (COOH) ₂	ν_{12}	C–H Out-of-plane
				997 ^d	<i>p</i> -C ₆ H ₄ (COOH) ₂	ν_{17a}	C–H Out-of-plane
973	977 ^c , 978 ^e	C ₆ H ₅ (COOH)	ν_{17a}	C–H Out-of-plane
				967 ^d , 962 ^e	<i>o</i> -C ₆ H ₄ (COOH) ₂	ν_{10a}	C–H Out-of-plane

Notes.

^a Only new absorption features and those present in the residue are reported as product peaks; the infrared spectrum of the ice was analyzed at 180, 250, and 300 K due to carbon dioxide (CO₂) and other light carbon subliming before 98 K and benzene (C₆H₆) subliming before 180 K, with 250 K being the residue formed by heavy irradiation products.

^b Bennett et al. (2010).

^c Stepanian et al. (1996).

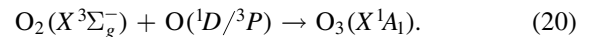
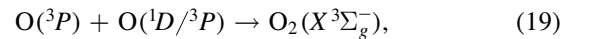
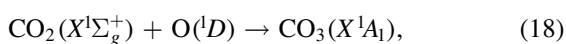
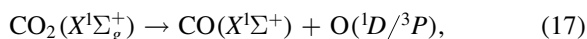
^d Arenas & Marcos (1980).

^e Brittain (2009).

^f Hollauer et al. (2001).

an order of magnitude of error when the column density is calculated. For the dicarboxylic acid, the addition of two carbon dioxide molecules proceeded with rate constants of $k_2 = (1.7 \pm 1.0) \times 10^{-4} \text{ s}^{-1}$ and $k_3 = (9.3 \pm 8.9) \times 10^{-6} \text{ s}^{-1}$, with the second addition proceeding at a lower rate than the first most likely due to the highly electronegative –COOH group, which limited the reactivity of the radical.

In addition to the targeted benzene carboxylic acid products, the column density evolution of carbon monoxide (CO), carbon trioxide (CO₃), and ozone (O₃) was monitored throughout the irradiation. Based on previous studies on irradiated carbon dioxide ices (Bennett et al. 2010), we propose the formation pathways for the aforementioned species to be



It is to be noted that some of these reactions require intersystem crossing. From the above reactions, we find that carbon dioxide is destroyed by means of reaction (17), yielding a carbon monoxide molecule and an oxygen atom. The released oxygen atom may be in either the excited singlet state (¹D) or the triplet ground state (³P). The pathway is endoergic by 532 kJ mol⁻¹ (5.51 eV) for the triplet channel and by 732 kJ mol⁻¹ (7.59 eV) for the singlet channel. The necessary energies to complete these reactions are supplied by the energetic electrons. From the electron fluence of $4.8 \times 10^{14} \text{ electron cm}^{-2}$, it can be determined that each electron initiates the destruction of 24 ± 8 carbon dioxide molecules—a process that requires $130 \pm 40 \text{ eV electron}^{-1}$ and $180 \pm 60 \text{ eV electron}^{-1}$ for the

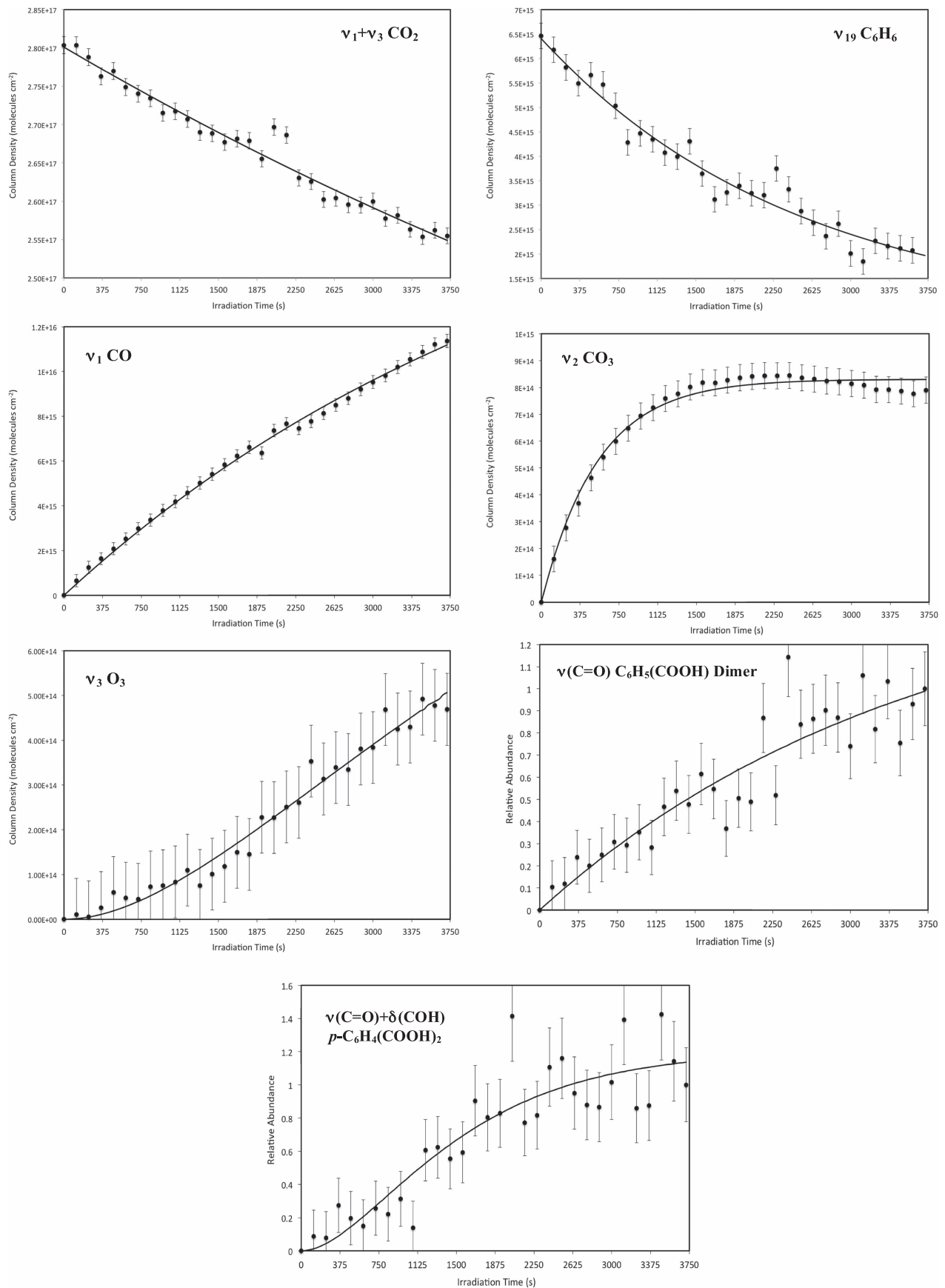


Figure 3. Fit of temporal (integrated infrared absorption) evolution of the two starting materials benzene (C₆H₆) and carbon dioxide (CO₂), benzoic acid (C₆H₅(COOH)), *para*-benzene dicarboxylic acid (C₆H₄(COOH)₂), and the newly formed light irradiation products carbon monoxide (CO), carbon trioxide (CO₃), and ozone (O₃) throughout the 1 hr irradiation period.

formation of ground- and excited-state oxygen atoms, respectively. These released suprathermal oxygen molecules may then react with unprocessed carbon dioxide molecules to produce carbon trioxide (reaction (15)). These processes can be modeled by the one-step $A' \rightarrow B'$ fitting:

$$[\text{CO}]_t = c(1 - e^{-k_4 t}) \quad (21)$$

$$[\text{CO}_3]_t = d(1 - e^{-k_5 t}). \quad (22)$$

Collectively, we find that the formation of carbon monoxide from reaction (14) and carbon trioxide from reaction (15) has rate constants of $k_4 = (2.1 \pm 0.2) \times 10^{-4} \text{ s}^{-1}$ and $k_5 = (1.84 \pm 0.07) \times 10^{-3} \text{ s}^{-1}$, respectively. Excess oxygen atoms produced from reaction (14) may react by way of reaction (16) to form molecular oxygen (O_2). In the second process, the newly formed molecular oxygen may react with a third atomic oxygen to produce ozone (O_3) based on the pathway depicted in reaction (17). Both of the aforementioned reaction pathways can occur with atomic oxygen in its excited singlet state (1D) or its triplet ground state (3P) due to the processes lacking entrance barriers and being exoergic by $498.5 \text{ kJ mol}^{-1}$ (5.167 eV) and $106.5 \text{ kJ mol}^{-1}$ (1.104 eV) for reactions (16) and (17), respectively. Considering a consecutive $A'' \rightarrow B'' \rightarrow C''$ reaction scheme, the temporal evolution was modeled by the following consecutive pseudo-first-order kinetics:

$$[\text{O}_3]_t = d \left(1 - \frac{k_7}{k_7 - k_6} e^{-k_6 t} - \frac{k_6}{k_7 - k_6} e^{-k_7 t} \right). \quad (23)$$

From the fittings, we find that reactions (16) and (17) have rate constants of $k_6 = (3.7 \pm 0.6) \times 10^{-4} \text{ s}^{-1}$ and $k_7 = (4.1 \pm 0.6) \times 10^{-4} \text{ s}^{-1}$, respectively.

5. ASTROPHYSICAL IMPLICATIONS

The present study demonstrates the formation of benzene carboxylic acids in icy mixtures of benzene and carbon dioxide (1:50) upon exposure to energetic electrons. Specifically, the species unambiguously identified in this study—benzoic acid and *meta*- and *para*-benzene dicarboxylic acid—align with those previously identified in the Murchison (Pizzarello et al. 2004; Pizzarello & Huang 2005) and Tagish Lake (Pizzarello et al. 2001) meteorites—namely, benzoic acid and the three benzene dicarboxylic acids. We expand upon these qualitative findings by modeling the mechanism for benzene carboxylic acid formation using a study on the formation of generic alkyl carboxylic acids (RCOOH) in interstellar model ices as a guideline (Kim & Kaiser 2010). Previous research on this topic postulates that carboxylic acid formation goes through a hydroxycarbonyl (HOCO) radical intermediate which is formed through the reaction of carbon dioxide (CO_2) and a suprathermal hydrogen atom. In this study, the hydrogen atoms are supplied via hydrogen loss from the benzene ring, forming a benzyl radical. The newly formed benzyl and HOCO radicals then undergo radical–radical recombination to yield a benzene carboxylic acid, i.e., benzoic acid (Figure 4). Through *in situ* infrared spectroscopy, the formation of radiation-induced mono- and disubstituted carboxylic acids was monitored, and optimized kinetic fittings were obtained. From this, the rate constant for the addition of a single carboxyl group was determined to be $(2.8 \pm 1.1) \times 10^{-4} \text{ s}^{-1}$, comparable to the

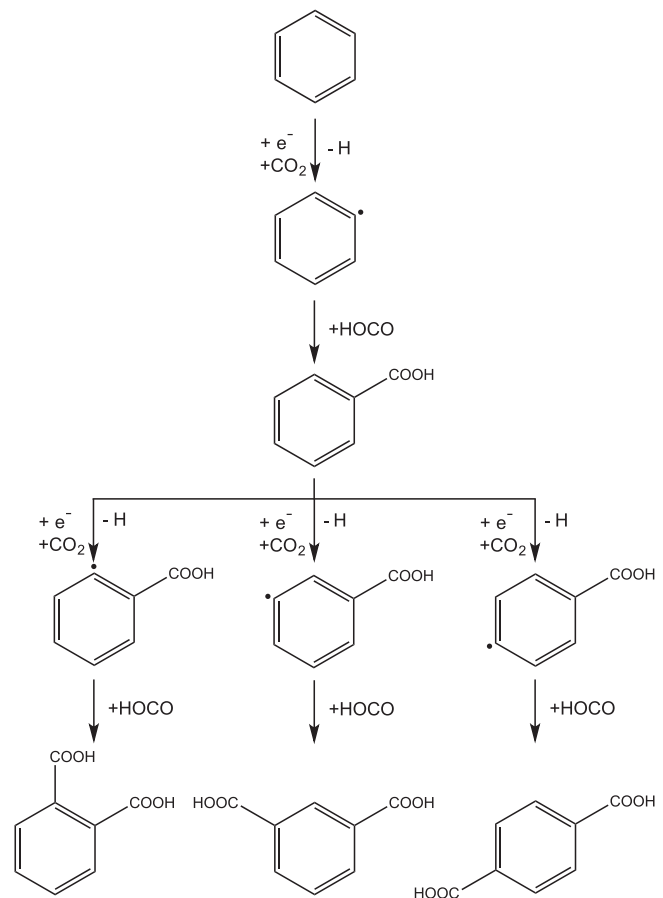


Figure 4. Reaction scheme used to fit the temporal evolution of the identified benzene carboxylic acids.

$1.1 \times 10^{-4} \text{ s}^{-1}$ found for the formation of generic alkyl carboxylic acids in hydrocarbon–carbon dioxide ice mixtures (Kim & Kaiser 2010). The addition of a second carbon dioxide molecule to benzoic acid was found to proceed at a rate of $(9.3 \pm 8.9) \times 10^{-6} \text{ s}^{-1}$, slower than the initial addition of carbon dioxide due to the effects of the highly electronegative carboxyl group. Since complex carboxylic acids ranging from succinic acid to glutaric acid—including benzoic acid ($\text{C}_6\text{H}_5\text{COOH}$)—were detected in Murchison, Orgueil, and Tagish Lake (Remusat et al. 2005), our laboratory experiments present a viable route to the formation of benzoic acid ($\text{C}_6\text{H}_5\text{COOH}$) in extraterrestrial ices. However, it should be noted that the model ice utilized in this study is not compositionally identical to interstellar ices and further experiments with more complex ices—such as those including water—are necessary. This study serves as a proof-of-concept to map possible formation routes of benzene carboxylic acids in analogous ices. Further astrochemical models incorporating non-equilibrium chemistry and rate constants as provided here should be established to quantify the formation of benzoic acid ($\text{C}_6\text{H}_5\text{COOH}$) on interstellar grains to better understand the synthesis of complex organic molecules of astrobiological relevance.

R.I.K. thanks the US National Science Foundation (AST-150550) for its support. The equipment was financed by the W. M. Keck Foundation.

REFERENCES

- Arenas, J., & Marcos, J. 1980, *AcSpA*, **36**, 1075
- Bennett, C. J., Hama, T., Kim, Y. S., Kawasaki, M., & Kaiser, R. I. 2011, *ApJ*, **727**, 27
- Bennett, C. J., Jamieson, C., Mebel, A. M., & Kaiser, R. I. 2004, *PCCP*, **6**, 735
- Bennett, C. J., Jamieson, C. S., & Kaiser, R. I. 2009, *ApJS*, **182**, 1
- Bennett, C. J., Jamieson, C. S., & Kaiser, R. I. 2010, *PCCP*, **12**, 4032
- Bennett, C. J., & Kaiser, R. I. 2007, *ApJ*, **660**, 1289
- Bernstein, M. P., Dworkin, J. P., Sandford, S. A., Cooper, G. W., & Allamandola, L. J. 2002a, *Natur*, **416**, 401
- Bernstein, M. P., Elsila, J. E., Dworkin, J. P., et al. 2002b, *ApJ*, **576**, 1115
- Brittain, H. G. 2009, *Cryst. Growth Des.*, **9**, 3497
- Brucato, J. R., Baratta, G. A., & Strazzulla, G. 2006, *A&A*, **455**, 395
- Câmara, J. S., Figueira, J., Perestrelo, R., Silva, C., & Pereira, J. 2014, in *Polyphenols: Food Sources, Bioactive Properties and Antioxidant Effects*, ed. D. T. Cobb (Hauppauge, NY: NOVA Science Publishers), 189
- Caro, G. M., Meierhenrich, U. J., Schutte, W. A., et al. 2002, *Natur*, **416**, 403
- Cernicharo, J., Heras, A. M., Tielens, A., et al. 2001, *ApJL*, **546**, L123
- Danger, G., Fresneau, A., Abou, M. N., et al. 2016, *GeCoA*, **189**, 184
- Drouin, D., Couture, A. R., Joly, D., et al. 2007, *J. Scanning Micro.*, **29**, 92
- Ehrenfreund, P., Bernstein, M., Dworkin, J., Sandford, S., & Allamandola, L. 2001, *ApJL*, **550**, L95
- Ehrenfreund, P., & Charnley, S. B. 2000, *ARA&A*, **38**, 427
- Elsila, J. E., Dworkin, J. P., Bernstein, M. P., Martin, M. P., & Sandford, S. A. 2007, *ApJ*, **660**, 911
- Gerakines, P. A., Schutte, W. A., Greenberg, J. M., & Van Dishoeck, E. F. 1995, *A&A*, **296**, 810
- Gibb, E., Whittet, D., Boogert, A., & Tielens, A. 2004, *ApJS*, **151**, 35
- Hollauer, E., Mondragon, M., & Castaño, V. M. 2001, *AcSpA*, **57**, 993
- Hollenberg, J. L., & Dows, D. A. 1962, *JChPh*, **37**, 1300
- Kaiser, R., & Roessler, K. 1997, *ApJ*, **475**, 144
- Kim, Y., & Kaiser, R. 2010, *ApJ*, **725**, 1002
- Koch, D. M., Toubin, C., Peslherbe, G. H., & Hynes, J. T. 2008, *JPC*, **112**, 2972
- Landera, A., Kaiser, R. I., & Mebel, A. M. 2011, *JChPh*, **134**, 024302
- Liu, S.-Y., Mehringer, D. M., & Snyder, L. E. 2001, *ApJ*, **552**, 654
- Martins, Z., Watson, J., Sephton, M., et al. 2006, *M&PS*, **41**, 1073
- McMurtry, B. M., Turner, A. M., Saito, S. E., & Kaiser, R. I. 2016, *JChPh*, **472**, 173
- Nuevo, M., Materese, C. K., & Sandford, S. A. 2014, *ApJ*, **793**, 125
- Oomens, J., Tielens, A., Sartakov, B. G., von Helden, G., & Meijer, G. 2003, *ApJ*, **591**, 968
- Parker, D. S., Zhang, F., Kim, Y. S., et al. 2012, *PNAS*, **109**, 53
- Pilling, S., Baptista, L., Boechat-Roberty, H. M., & Andrade, D. P. 2011, *AsBio*, **11**, 883
- Pizzarello, S. 2007, *OLEB*, **37**, 341
- Pizzarello, S., & Huang, Y. 2005, *GeCoA*, **69**, 599
- Pizzarello, S., Huang, Y., Becker, L., et al. 2001, *Sci*, **293**, 2236
- Pizzarello, S., Huang, Y., & Fuller, M. 2004, *GeCoA*, **68**, 4963
- Remijan, A., Snyder, L., Liu, S.-Y., Mehringer, D., & Kuan, Y.-J. 2002, *ApJ*, **576**, 264
- Remusat, L., Derenne, S., & Robert, F. 2005, *GeCoA*, **69**, 4377
- Rhee, Y. M., Lee, T. J., Gudipati, M. S., Allamandola, L. J., & Head-Gordon, M. 2007, *PNAS*, **104**, 5274
- Schidlowski, M. 1993, *The Chemistry of Life's Origins* (Berlin: Springer)
- Smith, K. E., Gerakines, P. A., & Callahan, M. P. 2015, *ChCom*, **51**, 11787
- Stepanian, S., Reva, I., Radchenko, E., & Sheina, G. 1996, *Vib. Spectrosc.*, **11**, 123
- Tielens, A. G. 2008, *ARA&A*, **46**, 289
- Whittet, D., Shenoy, S. S., Bergin, E. A., et al. 2007, *ApJ*, **655**, 332
- Zhou, L., Maity, S., Abplanalp, M., Turner, A., & Kaiser, R. I. 2014, *ApJ*, **790**, 38
- Zhou, L., Zheng, W., Kaiser, R. I., et al. 2010, *ApJ*, **718**, 1243
- Zuckerman, B., Ball, J. A., & Gottlieb, C. A. 1971, *ApJL*, **163**, L41